Journal of Materials Chemistry

Cite this: J. Mater. Chem., 2012, 22, 17284

www.rsc.org/materials

PAPER

Furan substituted diketopyrrolopyrrole and thienylenevinylene based low band gap copolymer for high mobility organic thin film transistors†

Prashant Sonar,*[a] Jing-Mei Zhuo,[b] Li-Hong Zhao,[c] Kai-Ming Lim,[b] Jihua Chen,[d] Adam J. Rondinone,[d] Samarendra P. Singh,[ae] Lay-Lay Chua,*[bc] Peter K. H. Ho[b] and Ananth Dodabalapur[af]

Received 17th April 2012, Accepted 19th June 2012
DOI: 10.1039/c2jm32376a

A novel solution processable donor–acceptor (D–A) based low band gap polymer semiconductor poly {3,6-difuran-2-yl-2,5-di(2-octyldodecyl)-pyrrolo[3,4-*c*]pyrrole-1,4-dione-*alt*-thienylenevinylene} (**PDPPF-TVT**), was designed and synthesized by a Pd-catalyzed Stille coupling route. An electron deficient furan based diketopyrrolopyrrole (DPP) block and electron rich thienylenevinylene (TVT) donor moiety were attached alternately in the polymer backbone. The polymer exhibited good solubility, film forming ability and thermal stability. The polymer exhibits wide absorption bands from 400 nm to 950 nm (UV-vis-NIR region) with absorption maximum centered at 782 nm in thin film. The optical band gap (E_g^{opt}) calculated from the polymer film absorption onset is around 1.37 eV. The π-energy band level (ionization potential) calculated by photoelectron spectroscopy in air (PESA) for **PDPPF-TVT** is around 5.22 eV. AFM and TEM analyses of the polymer reveal nodular terrace morphology with optimized crystallinity after 200 °C thermal annealing. This polymer exhibits p-channel charge transport characteristics when used as the active semiconductor in organic thin-film transistor (OTFT) devices. The highest hole mobility of 0.13 $cm^2 V^{-1} s^{-1}$ is achieved in bottom gate and top-contact OTFT devices with on/off ratios in the range of 10^6–10^7. This work reveals that the replacement of thiophene by furan in DPP copolymers exhibits such a high mobility, which makes DPP furan a promising block for making a wide range of promising polymer semiconductors for broad applications in organic electronics.

Introduction

Organic semiconductors are an important class of advanced functional materials for devices such as organic thin-film transistors (OTFTs), organic photovoltaics (OPVs), organic light emitting diodes (OLEDs), memory devices and chemical sensors.[1–5] The performance of these electronic devices depends strongly on the type of organic semiconductors used as the active layer with appropriate electrodes. These organic semiconducting materials could be either small molecules or polymers (homopolymers or copolymers).[6–8] Fabrication of these devices by printing requires materials which can be easily solution processed with optimum viscosity and ink formulation ability.[9] For such applications, polymers are generally preferable. In order to develop a good understanding of the structure–property–performance correlation and certain predictability of the properties of organic semiconductors, there are a few synthetic strategies in practice. Among these strategies, utilization of electron donating (D) and accepting (A) building blocks in the main polymer backbone appears to be one of the most simplistic, promising, attractive and successful strategies for both OTFT and OPV applications.[10–14] The presence of D and A conjugated blocks in the backbone of polymers causes reduction in the band gap *via* hybridization of the highest occupied molecular orbital (HOMO) [donor moiety] with the lowest unoccupied molecular orbital (LUMO) [acceptor moiety].[10] Such an alternate D–A arrangement also enhances the intermolecular and intramolecular interactions which directly govern the molecular ordering and π–π stacking of the polymer chains in the solid state. Among the reported D–A based copolymers, diketopyrrolopyrrole (DPP) based copolymers have shown faster growth for the realization of high performance in OTFT and

[a]*Institute of Materials Research and Engineering (IMRE), Agency for Science, Technology, and Research (A*STAR), 3 Research Link, Singapore 117602. E-mail: sonarp@imre.a-star.edu.sg; ananth.dodabalapur@engr.utexas.edu*
[b]*National University of Singapore, Department of Physics, Lower Kent Ridge Road, Singapore 117542. E-mail: chmcll@nus.edu.sg*
[c]*National University of Singapore, Department of Chemistry, Lower Kent Ridge Road, Singapore 117543*
[d]*Center for Nanophase Materials Sciences, Oak Ridge National Laboratory, Oak Ridge, TN 37831, USA*
[e]*School of Natural Sciences, Shiv Nadar University, Greater Noida, India*
[f]*Microelectronics Research Centre, The University of Texas at Austin, Austin, TX, 78758, USA*
† Electronic supplementary information (ESI) available. See DOI: 10.1039/c2jm32376a

OPV devices due to their fused planar aromatic core, strong electron withdrawing behaviour, suitable band gap engineering ability, thermal stability, mechanical properties and solution processability.[15–24] Additionally, the two carbonyl groups on the DPP moiety assist strong hydrogen bonding which reduces the π–π stacking distance. For the past two years, our group has been designing, synthesizing and studying the structure–property relationship of several DPP based solution processable D–A copolymers for OTFT and OPV devices.[25–28] Recently, an analogous compound of 3,6-di(thiophen-2-yl)pyrrolo[3,4-*c*]pyrrole-1,4(2*H*,5*H*)-dione (DBT), called 3,6-di(furan-2-yl)pyrrolo[3,4-*c*]pyrrole-1,4(2*H*,5*H*)-dione (DBF) (where thiophene units in the DBT block are replaced by furan), is becoming an interesting conjugated block for synthesising promising low band gap D–A copolymers and there are a few reports on the application of DBF based materials in organic electronics.[29–33] In our earlier published papers, we used DBF for making **PDBFBT**, **PDPP-FPF**, **PDPP-FNF** and **PDPP-FAF** copolymers and used them successfully in OTFT and OPV devices exhibiting higher performances.[31,33]

In this paper, we report the design, synthesis and characterization of another novel solution processable D–A based low band gap polymer semiconductor, poly{3,6-difuran-2-yl-2,5-di(2-octyldodecyl)-pyrrolo[3,4-*c*]pyrrole-1,4-dione-*alt*-thienylenevinylene} (**PDPPF-TVT**) comprised of an electron donating thienylenevinylene (TVT), more precisely dithienylehylene and an electron accepting DPP furan unit (Scheme 1). The choice of the TVT unit was anticipated to impart a strong electron donating ability due to the electron rich vinyl linkage. It has been reported that TVT based materials can demonstrate a high charge-carrier mobility as a consequence of a high planarity due to the vinylene (double bond character) group between two thiophene units.[34–36] The **PDPPF-TVT** copolymer was synthesized by a Pd-catalyzed Stille coupling route. We intentionally attached octyldodecyl as a long branched alkyl chain on both sides of the lactam nitrogen of the DBF unit in order to induce better solution processability. **PDPPF-TVT** is soluble in most of the common organic solvents such as chloroform, toluene and chlorobenzene and can be processed easily for making thin film devices. Morphological and microstructural properties of **PDPPF-TVT** have been studied by atomic force microscopy (AFM), X-ray diffraction (XRD) and transmission electron microscopy (TEM) analysis respectively. This polymer exhibits p-channel charge transport characteristics when used as the active semiconductor layer in OTFT devices. The highest hole mobility of 0.13 $cm^2 V^{-1} s^{-1}$ is achieved in bottom gate and top-contact OTFT devices with drain current on/off ratios in the range of 10^6–10^7. Earlier Kim *et al.* reported a hole mobility of 0.05 $cm^2 V^{-1} s^{-1}$ for poly{1,2-(*E*)-bis[2-(3-dodecyl-2-thienyl)-5-thienyl]ethene-*alt*-3,6-dithien-2-yl-2,5-di(2-ethylhexyl)-pyrrolo[3,4-*c*]pyrrole-1,4-dione} (PETVTDPP) in bottom contact top gate OTFT devices.[35] PETVTDPP is a comparable polymer semiconductor to **PDPPF-TVT**, where a dodecyl-thiophene unit attached to a TVT block is used in the conjugated backbone. To our knowledge, **PDPPF-TVT** is the first report of thienylenevinylene based copolymers with DPP that exhibit such a high mobility.

Results and discussion

The copolymer **PDPPF-TVT** was easily synthesized in four steps according to Scheme 1 using DBF and TVT conjugated moieties. First, compound 3,6-di(furan-2-yl)pyrrolo[3,4-*c*]pyrrole-1,4(2*H*,5*H*)-dione (**1**) was readily synthesized and isolated as an insoluble dark red-brownish powder with 60% yield by reacting 2-furylnitrile with diisopropyl succinate in the presence of sodium *tert*-amyl alcohol and iron chloride at 110 °C according to the published procedure.[31] The synthetic methodology is exactly similar to the preparation of 3,6-di(thiophen-2-yl)pyrrolo[3,4-*c*]pyrrole-1,4(2*H*,5*H*)-dione (DBT) except for using 2-furylnitrile instead of thiophene-2-carbonitrile. Compound **1** was then alkylated using 2-octyldodecyl bromide in anhydrous dimethylformamide (DMF) solvent in the presence of potassium carbonate (K_2CO_3), producing 2,5-bis(2-octyldodecyl)-3,6-di(furan-2-yl)pyrrolo[3,4-*c*]pyrrole-1,4(2*H*,5*H*)-dione with 40% yield. The attachment of an octyldodecyl branched alkyl group on lactam nitrogen atoms of the DPP core results in easy solution processability and this is convenient for easy purification by column chromatography. Bromination of 2,5-bis(2-octyldodecyl)-3,6-di(furan-2-yl)pyrrolo[3,4-*c*]pyrrole-1,4(2*H*,5*H*)-dione

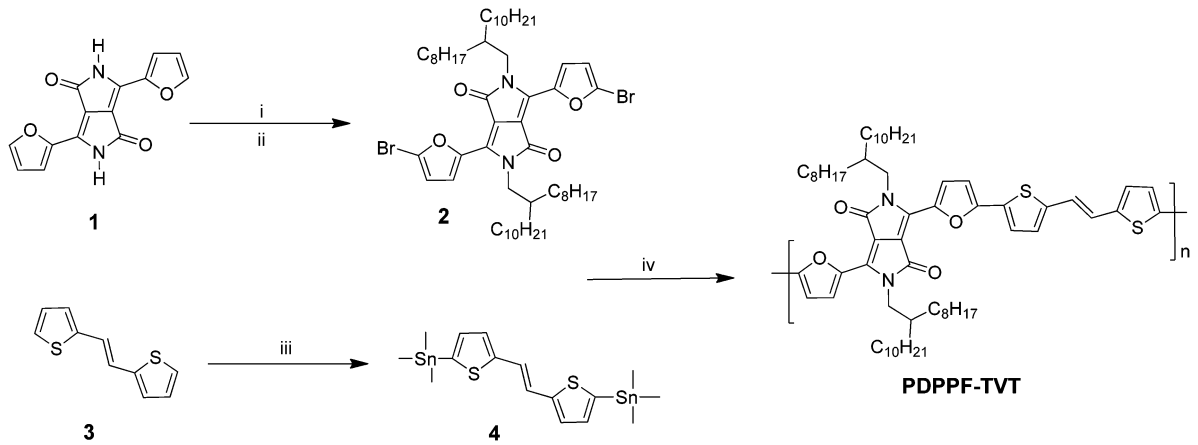

Scheme 1 *Reagents and conditions*: (i) K_2CO_3, 2-octyl-1-dodecyl bromide, anhydrous DMF, 120–130 °C, overnight 40%; (ii) bromine, chloroform, room temp., overnight, 73%; (iii) −78 °C, BuLi, TMEDA, trimethyltin chloride, THF–hexane, −78 °C for 20 h, 55%; (iv) $Pd(PPh_3)_2Cl_2$, anhydrous toluene, 90 °C for 72 h, 82%.

using bromine in chloroform at room temperature yielded the compound 3,6-bis(5-bromofuran-2-yl)-2,5-bis(2-octyldodecyl) pyrrolo[3,4-*c*]pyrrole-1,4(2*H*,5*H*)-dione (**2**) with 73% yield after careful purification *via* column chromatography (see Fig. S1 and S3†). Another comonomer based on TVT moiety, (*E*)-1,2-bis(5-(trimethylstannyl)thiophene-2-yl)ethane (**4**) was synthesized with 55% yield at −78 °C in the presence of *n*-butyllithium, tetramethyleneethylenediamine (TMEDA) and trimethyltin chloride using the commercially available starting material (*E*)-1,2-di(thiophen-2-yl) ethane (**3**) according to an earlier report (see Fig. S2 and S3†).[36] Stille coupling polymerization of 3,6-bis(5-bromofuran-2-yl)-2,5-bis(2-octyldodecyl)pyrrolo[3,4-*c*]pyrrole-1,4(2*H*,5*H*)-dione (**2**) with (*E*)-1,2-bis(5-(trimethylstannyl)thiophene-2-yl)ethane (**4**) in the presence of $Pd(PPh_3)_2Cl_2$ catalyst in anhydrous toluene at 90 °C yielded the target polymer poly {3,6-difuran-2-yl-2,5-di(2-octyldodecyl)-pyrrolo[3,4-*c*]pyrrole-1,4-dione-*alt*-thienylenevinylene} (**PDPPF-TVT**) (Scheme 1) with 82% yield. In order to remove the oligomer fractions and catalytic impurities, the polymer was purified by precipitation into methanol, followed by Soxhlet extraction using methanol, acetone, hexane and finally chloroform. Finally the polymer was dissolved in chloroform, followed by precipitation from methanol. The molecular weight of the **PDPPF-TVT** polymer was determined by high temperature gel permeation chromatography (HT-GPC). The number average (M_n) and weight average molecular weight (M_w) are 13 187 and 29 000 g mol^{-1}, respectively, at a column temperature of 160 °C with 1,2,4-trichlorobenzene (TCB) as the eluent and polystyrene (PS) as the standard (see Fig. S4†). The polydispersity index (PDI) of the copolymer is 2.20 which is calculated from the ratio of M_w and M_n (see Fig. S4†). The thermal behaviour of the polymer was characterized by differential scanning calorimetry (DSC) and thermogravimetric analysis (TGA). TGA showed a 5% weight loss at 390 °C under nitrogen, indicating the high thermal stability of **PDPPF-TVT**. A bulk polymer sample was analyzed by DSC with temperatures up to 350 °C, but there were no thermal transitions observed (see Fig. S5†).

The optical characteristics of **PDPPF-TVT** were investigated by UV-vis-NIR absorption spectroscopy. The solution UV-vis-NIR spectra are obtained from **PDPPF-TVT** in chloroform ($CHCl_3$) and chlorobenzene (CB). The UV-vis-NIR spectra of polymer thin films are obtained using a 60 nm thick film spin-coated from $CHCl_3$ and CB on Spectrosil (Fig. 1). The polymer (both in solution and thin film) showed a broad absorption band from 400 nm to 950 nm. Shorter and longer wavelength peaks are attributed to the π–π* transition band and interchain charge transfer (ICT) between TVT (donor) and DBF (acceptor) moieties, respectively. **PDPPF-TVT** in chloroform exhibits absorption maximum (λ_{max}) at 763 nm along with a shoulder at 710 nm as shown in Fig. 1(a). **PDPPF-TVT** in chlorobenzene also exhibits λ_{max} at 763 nm but the intensity of the peak was lower than that of the chloroform solution (Fig. 1(b)). In both solid thin films, **PDPPF-TVT** shows absorption maximum (λ_{max}) at 782 nm which is 19 nm red-shifted compared to the solution measurement. Such a red-shift probably arises from the intermolecular interactions of the polymeric chain that occurred in thin film samples. Similar observations have been noted in earlier reports on DPP based polymers.[15,16] From the edge of the solid state absorption of **PDPPF-TVT** at 905 nm, the optical band gap (E_g^{opt}) was calculated as 1.37 eV. This optical band gap value is quite comparable with an earlier reported analogous PETVTDPP copolymer (1.43 eV).[35]

The HOMO energy level of **PDPPF-TVT** was calculated from photoelectron spectroscopy in air (PESA) data characterized by using a thin film of spin coated **PDPPF-TVT** on a glass substrate as shown in Fig. 2. The HOMO energy level was determined

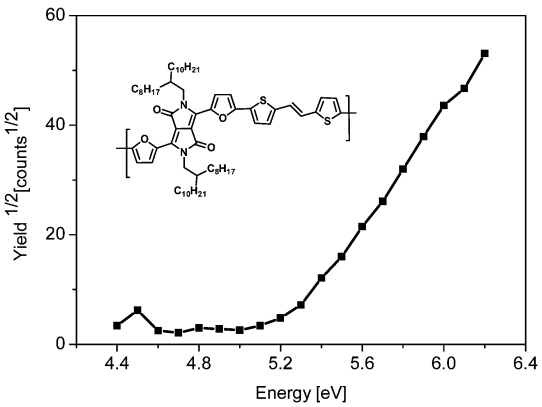

Fig. 2 Photoelectron spectroscopy in air (PESA) measurements of the **PDPPF-TVT** copolymer thin film spin coated on a glass substrate.

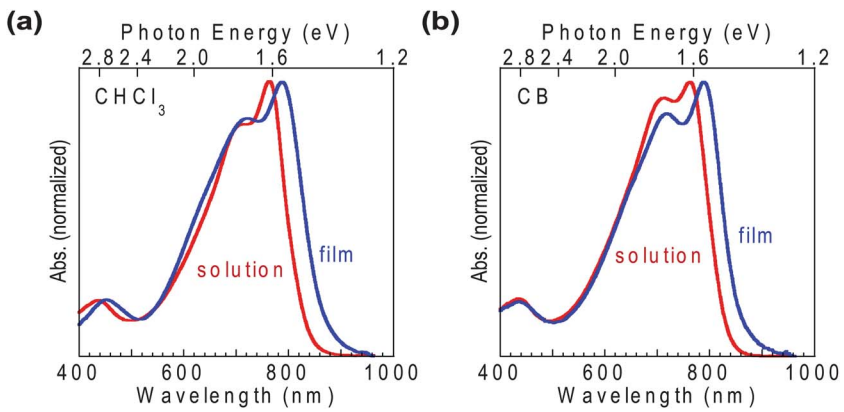

Fig. 1 Normalized UV-vis-NIR absorption spectra of **PDPPF-TVT**. (a) In chloroform ($CHCl_3$). (b) In chlorobenzene (CB). The red curve is in 0.01 mg mL^{-1} dilute solution. The blue curve is for thin film spin-coated from 5 mg mL^{-1} solution.

from the onset energy value to be 5.22 eV. This result suggests that this polymer is oxidatively stable, which is very important for manufacturing stable organic electronic devices. The LUMO level was estimated to be 3.81 eV calculated from the optical band gap and the HOMO level.

X-ray diffraction (XRD) measurements were carried out on the polymer flakes in order to determine the molecular packing and solid state ordering of the polymer. Polymer flakes were prepared by evaporating the solvent from a dilute polymer solution in chloroform to form a thick polymer film in the flask, followed by carefully washing off the film with methanol (a non-solvent for the polymer). The polymer flake was then cut into small pieces and used for 2D XRD measurements. The 2D XRD diffraction pattern and 2D XRD image for the perpendicular incidence of X-ray on the flakes of the **PDPPF-TVT** copolymer are shown in Fig. 3.

A diffractogram shown in Fig. 3 exhibits two peaks which correspond to interlayer *d*-spacing and π–π stacking respectively. The primary strong peak at $2\theta = 4.51°$ (θ is the diffraction angle) corresponds to the reflection of the crystal plane with an interlayer *d*-spacing of 19.96 Å. The broad secondary diffraction peaks for **PDPPF-TVT** range from $2\theta = 15$ to 30° suggesting that this copolymer possesses an amorphous nature. The broad peak reflects simply the short range intermolecular distance due to van der Waals force, which includes the π–π distance and the distance between other parts of the polymer chains such as side chains. Such a broad diffraction pattern and 2θ value were also observed for other DPP polymers such as PDBFBT, PDPP-FPF, PDPP-FNF, PDPP-FAF, PDTDPP-*alt*-EMD, C10-PPE-DPP, *p*-DPPS3 and Pdpps2TT respectively.[31,33,37,38] The distance estimated from the broad peak is 4.20–4.66 Å. Such a broad peak is most probably a signature of non-aligned polymer backbones. Variations in interlayer *d*-spacing and hence a broad diffraction peak arise from the differences in conjugated backbone planarity (torsion angle difference between DPP furan and TVT blocks) due to steric hindrance and D–A intramolecular–intermolecular interactions.

Bottom-gate, bottom contact 60 nm-thick OTFT devices were fabricated by spin coating 5 mg mL^{-1} **PDPPF-TVT** solution from chloroform or chlorobenzene on a self-assembled monolayer (SAM) of octadecyltrichlorosilane (OTS)–hexamethylsilazane (HMDS) treated Si/SiO_2 wafer. Generally appropriate SAM treatment controls the surface energy, induces molecular orientation and reduces the number of trapping sites for better charge transportation. The devices were then annealed at 150 °C, 200 °C, 250 °C and 300 °C on a hot plate for 15 min under dry nitrogen in order to study the effect of thermal annealing on charge carrier transport. These OTFT devices were characterized in a glove box under dry nitrogen using a Keithley 4200-SCS analyzer. The OTFT mobility as a function of annealing temperature is shown in Fig. 4.

Both CB and $CHCl_3$ devices showed p-channel field effect characteristics. The field-effect hole mobilities ($\mu_{p,FET}$) were extracted in the linear regime at $V_{DS} = -40$ V. The OTFT mobility increases for both CB and $CHCl_3$ devices as the annealing temperature increases from room temperature to 250 °C and decreases at temperatures beyond 250 °C. The optimal hole mobilities obtained with thermal annealing are 0.11 $cm^2\ V^{-1}\ s^{-1}$ and 0.06 $cm^2\ V^{-1}\ s^{-1}$ for chloroform and chlorobenzene devices respectively. A threshold voltage (V_T) = −16.0 V with a current on/off ratio (I_{on}/I_{off}) of ~10^6 was

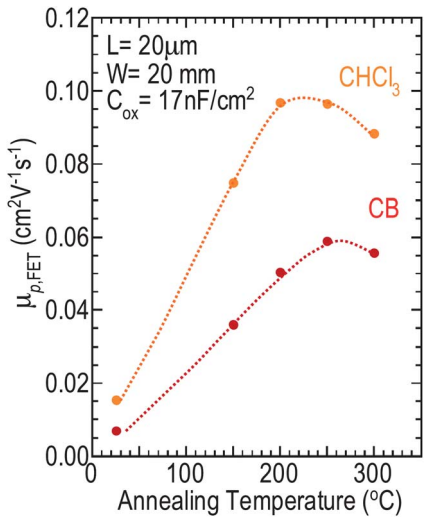

Fig. 4 Temperature dependence of field-effect mobility for devices spin-coated from chlorobenzene (CB) and chloroform ($CHCl_3$). Films have been annealed and quench-cooled.

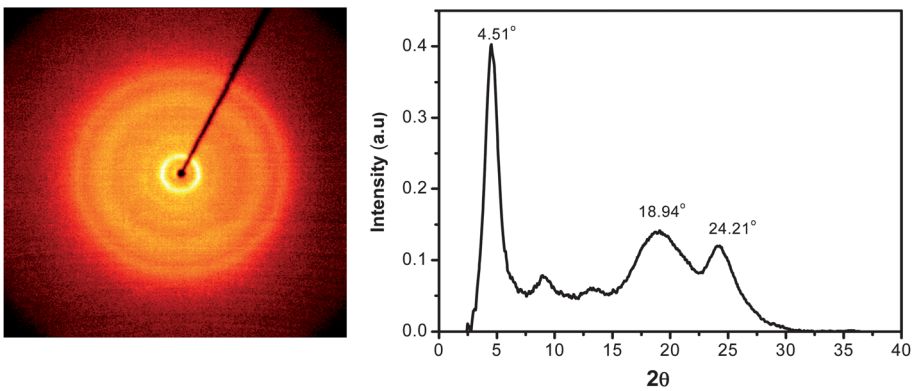

Fig. 3 2D XRD pattern intensity graphs (right) and 2D XRD image (left) obtained with the incident X-ray perpendicular to the thin film stack of the **PDPPF-TVT** copolymer.

observed. The higher OTFT mobility obtained for $CHCl_3$ devices are consistent with the UV-vis-NIR data. The $CHCl_3$ film gives more red-shifted order states. In addition, we have also studied the effect of quench-cooled and slow-cooled (after annealing) thin films of **PDPPF-TVT** processed in chloroform and chlorobenzene on OTFT performance respectively.

First, we preannealed a 60 nm thick film of **PDPPF-TVT** at 200 °C (chloroform processed) and 250 °C (chlorobenzene processed) for 15 min and then slowly cooled at a rate of 0.1 °C min^{-1} to 50 °C. OTFT devices exhibited the highest mobilities of 0.13 $cm^2 V^{-1} s^{-1}$ and 0.08 $cm^2 V^{-1} s^{-1}$ respectively for chloroform and chlorobenzene processed slowly cooled thin films, which showed a 30% increment in mobility compared to the quench-cooled samples. Both slow cooled and quench-cooled chloroform processed OTFT device characteristics are shown in Fig. 5. The slow-cooled and quench-cooled chlorobenzene processed OTFT device characteristics are shown in Fig. S5.† The higher mobility of slow-cooled devices compared to the quench-cooled samples may be due to better ordering of the polymeric chains due to slow cooling. Such a slow cooling allows sufficient time for the polymer chains to further relax to their preferred orientation. Further, temperature dependence of charge carrier mobility for the **PDPPF-TVT** polymer based OTFT was studied by measuring output and transfer characteristics in the range of 95–295 K. The field-effect hole mobilities extracted in the linear regime as a function of inverse temperature are shown in Fig. 6. The mobility–temperature characteristics exhibit a simple Arrhenius relationship with an apparent activation energy (E_a) of 58 meV. This E_a value is comparable to those of high mobility polymer semiconductor poly(2,5-bis(3-tetradecylthiophen-2-yl) thieno[3,2-b]thiophene (PBTTT) based OTFT devices.[39] The FET characteristics in both output and transfer plots are well-behaved over the entire temperature range with little hysteresis and voltage shift, hence the $\mu_{p,FET}$ values obtained are reliable.

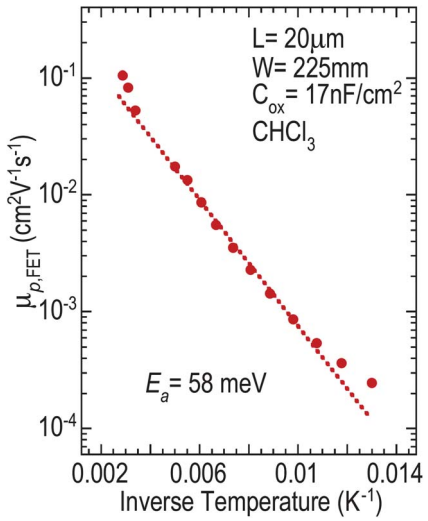

Fig. 6 Arrhenius plot of the temperature dependence of $\mu_{p,FET}$ taken during the warming up cycle. $\mu_{p,FET}$ was extracted at $V_{ds} = -20$ V in the linear regime.

We further show that the **PDPPF-TVT** film exhibits relatively good stability when exposed to air in light. We observed only a small gate threshold shift (VT) of *ca.* +5 V after 3-day of exposure as compared to the well-studied PBTTT (*ca.* +20 V) and regio-regular poly(3-hexylthiophene) (rr-P3HT) FET (*ca.* +40 V) OTFT devices.[39,40] The off current of rr-P3HT and PBTTT OTFT devices showed more than 4 orders of increment while for **PDPPF-TVT** devices we did not observe any off current enhancement. We also drive PBTTT and **PDPPF-TVT** OTFT in air and in the dark with on/off pulses of $V_{GS} = 0$ V and −60 V at $V_{DS} = -40$ V for 30 min [see Figure S8(a)–(c)†]. The source-drain current (I_{DS}) drops by approximately 2 times and 4 times for

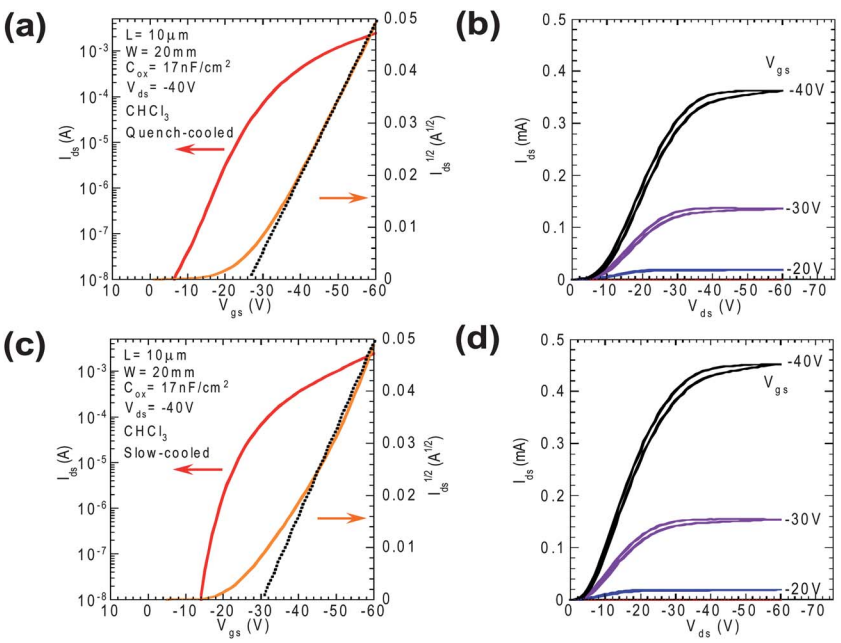

Fig. 5 Transfer and output characteristics for **PDPPF-TVT** FETs spin-coated from chloroform on OTS–HMDS-treated Si/SiO_2 substrates after annealing at 200 °C for 15 min. (a) and (b) Quench-cooled after annealing; (c) and (d) slow cooled at a rate of 0.1 °C min^{-1} to 50 °C.

PBTTT and PDPPF-TVT respectively for the first 20 min and levels off. These experiments suggest that **PDPPF-TVT** has a relatively stable photo-doping stability compared to PBTTT and rr-P3HT films [see Figure S8(d)†]. This is most likely due to the lower IP of **PDPPF-TVT**.

Atomic force microscopy (AFM) measurements were undertaken to visualize the morphological changes with respect to the increasing annealing temperature. The surface morphology of the 60 nm thick film subjected to different annealing conditions is shown in the AFM images of Fig. 7. Pristine films displayed nodular morphology which is typically observed for high molecular weight semicrystalline conjugated polymer thin films.[41,42] The AFM images clearly show a slight change in morphology with annealing. At room temperature domains look less pronounced but as the annealing temperature increases the domains are more visible and become interconnected.

As the annealing temperature increases, polymer chains start to crystallize and form smaller, more densely packed crystalline grains. For a comparative study, AFM analysis was also conducted on chlorobenzene processed thin films (see Fig. S6†).

We also conducted transmission electron microscopy (TEM) analysis by depositing drop cast films of **PDPPF-TVT** on carbon coated grids. TEM images and corresponding selected area electron diffraction (SAED) patterns for **PDPPF-TVT** films at room temperature and annealed at various temperatures (same as those used for OTFT device fabrication) are shown in Fig. 8 and 9 respectively.

Similar to the AFM results, bright-field TEM images show that films fabricated from chloroform solution exhibit a nodular structure. A slight elongation of the nodular structure was visible for as-cast films and the films annealed at 150 °C and 200 °C.

Thermal annealing at 150 °C or 200 °C increased the sharpness of the 0.43 nm reflection in SAED patterns and an additional ring appears at 200 °C annealing temperature, which suggests

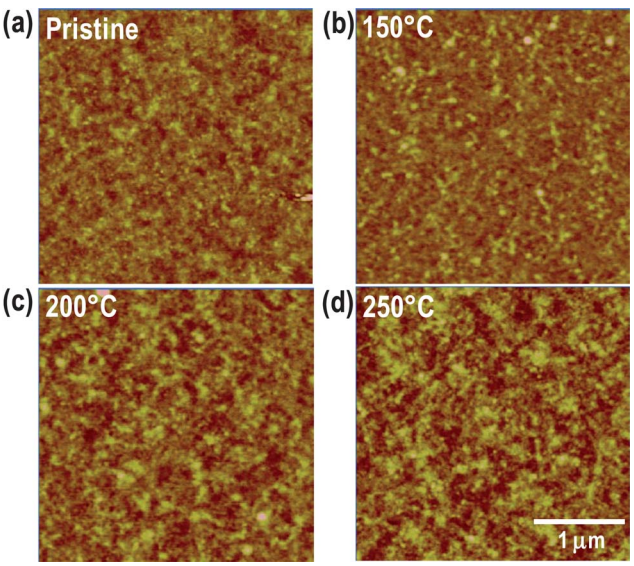

Fig. 7 AFM images of the 60 nm thick film spin-coated from chloroform on an OTS–HMDS-treated native Si substrate. (a) As-cast film. Films annealed at (b) 150 °C; (c) 200 °C and (d) 250 °C for 15 min. The scale bar denotes 1 μm. *z*-height = 14 nm.

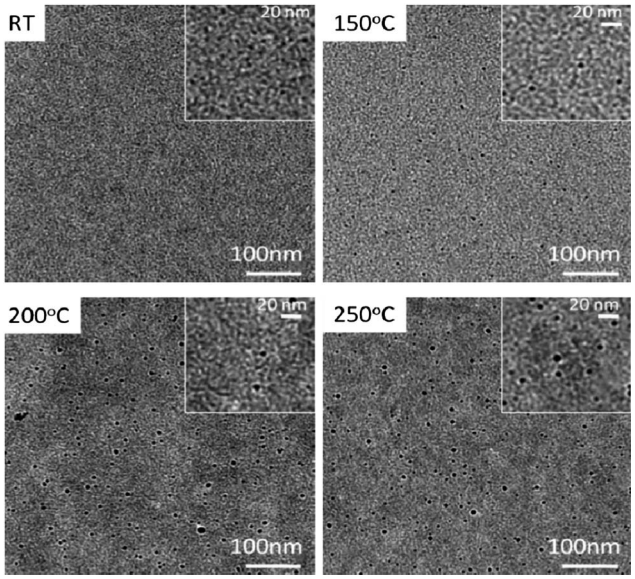

Fig. 8 TEM images of **PDPPF-TVT** (a) as-cast film. Films annealed at (b) 150 °C; (c) 200 °C and (d) 250 °C for 15 min.

significantly enhanced crystallinity and corresponds well to the optimized hole transport. The outer ring in the SAED pattern of the film after 200 °C annealing corresponds to a *d* spacing of 0.36 nm, which is probably correlated with the π–π stacking distance of the **PDPPF-TVT** chains. Annealing at 250 °C degraded the crystallinity and the 0.36 nm ring in SAED is blurred; this observation conforms well with a reduced hole mobility in OTFT devices at this temperature. Films fabricated from chlorobenzene solution generally exhibit more nanofiber-type features and stronger SAED reflections than the ones from chloroform solution, likely caused by the higher boiling point of chlorobenzene (see Fig. S7†). Although slow evaporation allows polymer chains to aggregate,[43] the resultant nanofibers likely

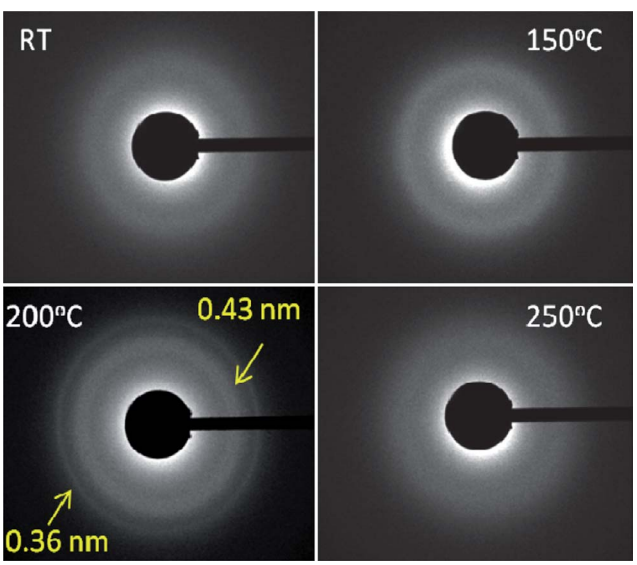

Fig. 9 SAED patterns of **PDPPF-TVT** (a) as-cast film. Films annealed at (b) 150 °C; (c) 200 °C and (d) 250 °C for 15 min.

introduce a considerable amount of defects between the nanofibers, which lead to slightly less effective charge transport in these films as compared to the films fabricated from chloroform solution. For films fabricated from both chloroform and chlorobenzene solutions, the crystallinity trend revealed from SAED patterns is consistent with the observed OTFT performance at different annealing temperatures.

Conclusions

In summary, we have reported a novel DPP furan and thienylenevinylene based donor–acceptor solution processable polymer semiconductor **PDPPF-TVT** *via* Stille coupling. The polymer showed good solubility, film forming ability and wide absorption in the UV-vis-NIR region. Optical band gap and HOMO values reveal the lower band gap nature of the polymer and that it is a stable material for organic electronic devices. Bulk and surface morphology characterized by AFM and TEM analysis of the polymer reveals nodular terrace morphology. After annealing, the effects of quench- and slow-cooling of polymeric thin films on charge transport properties were investigated. Highest field-effect hole mobilities of 0.13 $cm^2\ V^{-1}\ s^{-1}$ and 0.078 $cm^2\ V^{-1}\ s^{-1}$ were obtained in chloroform and chlorobenzene processed thin films in OTFT devices respectively with current on/off ratios in the range of 10^6–10^7. Such high mobility values arise from the strong intermolecular interactions and favorable π–π stacking of fused aromatic DPP and thienylenevinylene conjugated blocks. Our study in this work clearly shows that the furan substituted DPP is a promising building block for synthesising various donor–acceptor low band gap conjugated materials for high performance OTFT devices. This polymer is a potential candidate for organic phototransistors and other organic electronic devices.

Experimental

General

Most of the chemicals were purchased from Sigma-Aldrich, Strem and Acros and used without further purification. All reactions were conducted using Schlenk techniques under an argon or nitrogen atmosphere with anhydrous solvents. 3,6-Di(furan-2-yl)pyrrolo[3,4-*c*]pyrrole-1,4(2*H*,5*H*)-dione (DBF core) and (*E*)-1,2-bis(5-trimethylstannyl)thiophen-2-yl-ethene were synthesized according to the literature method.[31,36]

Instrumentation and characterization

^1H and ^{13}C NMR data were recorded in $CDCl_3$ solvent on a Bruker DPX 400 MHz spectrometer and chemical shifts were measured in ppm. Matrix assisted laser desorption/ionization time-of-flight (MALDI-TOF) mass spectra were obtained on a Bruker Autoflex TOF/TOF instrument. HT-GPC measurements were performed on a Polymer Labs GPC-220 equipped with a refractive index detector, a 500 μm injection loop, two PLgel Olexis columns (300 mm × 7.5 mm, particle size: 13 μm) and one PLgel Olexis 13 μm guard column (50 mm × 7.5 mm) at 160 °C using 1,2,4-trichlorobenzene stabilized with 0.0125 g L^{-1} BHT as the eluent. Polymer solutions were prepared at a concentration of 0.3 mg mL^{-1} using a Polymer Labs SP260 sample preparation system at 160 °C for 1 min, which resulted in complete dissolution of the polymers, followed by transfer to the GPC vials. The measured data were analyzed with Cirrus software, using narrow MWD polystyrene standards as a reference (PL EasiVial PS, range of calibration 103 to 6×10^6). UV-vis-NIR spectra were recorded on a Shimadzu model 2501-PC using 0.01 mg mL^{-1} of **PDPPF-TVT** solution in chloroform and chlorobenzene. These solutions were heated at 55 °C for 15 min before measurement and thin films were spin coated on Spectrosil for solid state measurement. The photoelectron spectroscopy in air (PESA) measurement was done on the thin film of **PDPPF-TVT** polymer spin coated on glass using a Riken Photoelectron Spectrometer (Model AC-2). Differential scanning calorimetry (DSC) was carried out under nitrogen on a TA Instrument DSC Q100 instrument (scanning rate of 10 °C min^{-1}). Thermogravimetric analysis (TGA) was carried out using a TA Instrument TGA Q500 instrument at a heating rate of 10 °C $min.^{-1}$ 6.24 mg mL^{-1} and 5.0 mg mL^{-1} of **PDPPF-TVT** polymer in chloroform and chlorobenzene were dissolved and the solution was heated at 55 °C for 15 min and then cooled for another 15 min before spin coating onto four OTS treated native substrates. Substrates were annealed to individual temperatures for 15 min in N_2 and then either quench-cooling or slow cooling was carried out. These thin film deposited substrates were used for atomic force microscopy (AFM) measurements. AFM images were recorded with a Nanoscope V microscope (Veeco Inc., Santa Barbara, CA) operated in tapping mode at room temperature in air, using microfabricated cantilevers (spring constant of 30 N m^{-1}). The images were recorded with a 1024 pixel resolution in each direction and are shown as captured. Thermal annealing was carried out on thin film samples at 150 °C, 200 °C, 250 °C and 300 °C for 15 min in nitrogen. **PDPPF-TVT** samples for two-dimensional X-ray diffraction (2D XRD) measurements were measured on the polymer flakes using a Bruker AXS D8 system with a Cu K_α source in air. Data were analyzed with the GADDS software. TEM samples were examined with a Zeiss Libra 120 at 120 kV. Bright field images were taken at a consistent defocus of 2 microns, and selected area electron diffraction (SAED) patterns were collected with a 500 nm diameter aperture and a camera length of 576 mm. SAED patterns were calibrated against an aluminum standard assuming the Al (111) *d*-spacing of 0.234 nm.

Synthesis of 3,6-di(furan-2-yl)pyrrolo[3,4-*c*]pyrrole-1,4(2*H*,5*H*)-dione (1). Sodium (5.17 g, 0.225 mol) was added to a three-neck flask containing 2-methyl-1-butanol (90 mL) under argon. The mixture was heated to 90 °C and $FeCl_3$ (65 mg) was added. After the complete disappearance of sodium, the solution was cooled to 85 °C. 2-Furonitrile (13.96 g, 0.15 mol) was added to the reaction mixture, followed by the dropwise addition of diisopropyl succinate (12.15 g, 0.06 mol) in 2-methyl-1-butanol (8 mL) over 1 h at 85 °C. When the addition was completed, the mixture was stirred for an additional 2 h at this temperature. The reaction mixture was then cooled to 50 °C, diluted with methanol (65 mL), and then slowly neutralized with glacial acetic acid (~25 mL) and refluxed for 15 min. The reaction mixture was cooled down to room temperature and filtered. The solid was washed respectively with hot methanol and de-ionized (DI) water several times, and dried *in vacuo* at 50 °C. A dark red solid was

obtained. Yield: 9.00 g (60.0%). ^{1}H NMR (300 MHz, DMSO-d_6): δ 11.17 (s, 2H), 8.04 (d, $J = 1.3$ Hz, 2H), 7.65 (d, $J = 3.4$ Hz, 2H), 6.83 (dd, $J = 1.3$ Hz, 3.4 Hz, 2H). ^{13}C NMR (75 MHz, DMSO-d_6): δ 107.57, 113.71, 116.79, 131.27, 143.75, 146.91, 161.71.

Synthesis of 3,6-bis(5-bromofuran-2-yl)-2,5-bis(2-octyl-1-dodecyl)pyrrolo[3,4-*c*]pyrrole-1,4(2*H*,5*H*)-dione (2). Compound **1** (4.0 g. 14.90 mmol) and anhydrous K_2CO_3 (6.17 g, 44.70 mmol) were added to a dry 250 mL three-neck round bottom flask, and kept under vacuum at 50 °C for one hour, then anhydrous *N*,*N*-dimethylformamide (DMF) (300 mL) was added under argon to the above mixture. This mixture was then heated to 120 °C under argon for 1 h. 2-Octyl-1-dodecylbromide (16.15 g, 44.70 mmol) was added dropwise, and the reaction mixture was further stirred overnight at 130 °C. The reaction mixture was allowed to cool down to room temperature the next day and poured into water (600 mL) and stirred for 30 min. The product was extracted with chloroform, washed with DI water, and dried over anhydrous $MgSO_4$. Removal of the solvent afforded the crude product which was further purified using column chromatography on silica gel (a mixture of hexane and chloroform as the eluent) to give the product as a red solid (5.0 g, 40%). M.p. (DSC): 110.5 °C. ^{1}H NMR (400 MHz, $CDCl_3$): δ 0.86 (t, $J = 6.4$ Hz, 12H), 1.15–1.40 (m, 64H), 1.79 (s, 2H), 4.01 (m, 4H), 6.68 (dd, $J = 1.4$ Hz, 1.6 Hz, 2H), 7.59 (s, 2H), 8.32 (d, $J = 3.6$ Hz, 2H). ^{13}C NMR (100 MHz, $CDCl_3$): δ 160.89, 146.25, 132.82, 126.16, 122.17, 115.48, 106.36, 46.65, 38.80, 31.90, 31.87, 31.48, 30.09, 29.62, 29.61, 29.54, 29.49, 29.32, 29.27, 26.48, 22.65, 22.63, 14.05. MS (MALDI-TOF, *m*/*z*): calcd. for $C_{54}H_{88}N_2O_4$, 828.67; found, 828.53 (*M*).

2,5-Bis(2-octyl-1-dodecyl)-3,6-di(furan-2-yl)pyrrolo[3,4-*c*]pyrrole-1,4(2*H*,5*H*)-dione (4.0 g, 4.82 mmol) and chloroform (40 mL) were charged into a 100 mL three neck flask equipped with a stirring bar, a condenser, and a dropping funnel. Bromine (Br_2) (0.50 mL, 9.64 mmol) in chloroform (20 mL) was then added dropwise to the flask at room temperature through the dropping funnel. The mixture was stirred at room temperature overnight, then slowly poured into an aqueous solution of sodium thiosulfate and stirred for additional 30 min. The product was extracted with chloroform, then washed with DI water, and dried over anhydrous $MgSO_4$. Removal of the solvent afforded the crude product which was further purified using column chromatography on silica gel (a mixture of hexane and chloroform as the eluent) to give the product as a dark red solid (3.50 g, 73%). M.p. (DSC): 105.0 °C. ^{1}H NMR (400 MHz, $CDCl_3$): δ 0.85 (t, $J = 6.2$ Hz, 12H), 1.10–1.40 (m, 64H), 1.76 (s, 2H), 3.96 (d, $J = 6.7$ Hz, 4H), 6.59 (d, $J = 3.4$ Hz, 2H), 8.27 (d, $J = 3.4$ Hz, 2H). ^{13}C NMR (100 MHz, $CDCl_3$): δ 160.87, 146.23, 132.78, 126.13, 122.14, 115.45, 106.34, 46.63, 38.78, 31.87, 31.84, 31.47, 30.07, 29.59, 29.52, 29.46, 29.29, 29.24, 26.46, 22.62, 14.02. MS (MALDI-TOF, *m*/*z*): calcd. for $C_{54}H_{86}Br_2N_2O_4$, 987.08; found, 986.38.

Synthesis of (*E*)-1,2-bis(5-trimethylstannyl)thiophen-2-yl-ethene (4). To a solution of *trans*-1,2-di(2-thienyl)ethylene (1.78 g, 9.26 mmol) in tetrahydrofuran (THF)/hexane (2 : 1, 50 mL), tetramethylethylenediamine (TMEDA) (3.10 mL, 20.7 mmol) was added at −50 °C, and then 2.0 M solution of *n*-butyllithium in cyclohexane (11.0 mL, 22.0 mmol) was added dropwise at −78 °C. The mixture was then refluxed at 100 °C for 1 h. The reaction solution was cooled to −78 °C and a 1.0 M solution of trimethyltin chloride in THF (22.0 mL, 22.0 mmol) was added. The solution was warmed to room temperature (rt) and stirred overnight. The crude component was poured into water (150 mL) and diethyl ether (200 mL). The organic phase was then separated, dried over magnesium sulfate ($MgSO_4$) and the solvent was evaporated under reduced pressure. It was recrystallized from ethanol (150 mL) to give (*E*)-1,2-bis(5-trimethylstannyl)thiophen-2-yl-ethene as a gray crystalline solid (55% yield).

^{1}H NMR (400 MHz, $CDCl_3$): δ 0.36 (s, 18H), 7.07 (d, 2H), 7.08 (d, 2H), 7.11 (d, 2H). ^{13}C NMR (100 MHz, $CDCl_3$): δ 148.63, 137.92, 136.16, 128.04, 127.42, 127.22, 126.37, 124.68, 121.61, −7.87. MS (MALDI-TOF, *m*/*z*): calcd. for $C_{54}H_{86}Br_2N_2O_4$, 517.91; found, 517.86.

Synthesis of poly{3,6-difuran-2-yl-2,5-di(2-octyldodecyl)-pyrrolo[3,4-*c*]pyrrole-1,4-dione-*alt*-thienylenevinylene} (PDPPF-TVT). To a Schlenk flask, 3,6-bis(5-bromofuran-2-yl)-2,5-bis(2-octyl-1-dodecyl)pyrrolo[3,4-*c*]pyrrole-1,4(2*H*,5*H*)-dione (**2**) (0.350 g, 0.35 mmol), (*E*)-1,2-bis(5-trimethylstannyl)thiophen-2-yl-ethene (**4**) (0.181 g, 0.35 mmol), and bis-(triphenylphosphine)palladium(II) dichloride (14 mg, 0.02 mmol) were added and kept under vacuum for 15 min and then vacuum–argon cycles were repeated three times. Then anhydrous toluene (15 mL) was added and the solution was purged with argon for 30 min. The reaction mixture was heated to 90 °C and stirred for 48 h. Bromobenzene (0.5 mL) was added to the reaction mixture for further reaction with the residual trimethylstannyl end group. The mixture was further stirred at 90 °C for 8 h before cooling down to room temperature. The mixture was then poured into stirring methanol (200 mL), filtered off, washed with methanol, and dried. The solid was then further purified by Soxhlet extraction using acetone (24 h), hexane (24 h), and then dissolved with chloroform. Yield: 0.290 g (82%). GPC (at 40 °C; THF + chloroform as the eluent; polymethylmethacrylate as the standard). M_w/M_n (GPC) = 455 300/219 600, polydispersity index (PDI) = 2.07, λ_{max} (UV-vis-Near IR): 763 nm (in chloroform); 782 nm (thin film).

OTFT device fabrication and characterization

Bottom gate bottom contact OTFT devices were fabricated using thin films of **PDPPF-TVT** (~60 nm) on octadecyltrichlorosilane (OTS)–hexamethyldisilazane (HMDS) treated [the wafer was treated with OTS in the solution phase (0.1 mM, in HPLC-grade toluene, 25 °C) for 2 h in a N_2-purged glove box to form a close-packed monolayer; the OTS-modified surface was then further treated with vapour HMDS (120 °C) for 10 min to terminate all unreacted silanol groups] 200 nm SiO_2 substrates by spin-coating a polymer solution in chloroform (6 mg mL^{-1}) or chlorobenzene (5 mg mL^{-1}). We then measured field effect mobility for these cast film and films annealed at 150 °C, 200 °C, 250 °C and 300 °C for 15 min respectively in a nitrogen purged environment. Evaluation of OTFTs was carried out in a glove box under nitrogen using a Keithley 4200 parameter analyzer. The field-induced hole mobility ($\mu_{p,FET}$) was calculated from the data in the linear regime (gate voltage, V_{GS} > source–drain voltage, V_{DS})

according to the equation: $\mu_{p,FET} = I_{SD}L/WC_iV_{DS}/(V_{GS} - V_T)$, where I_{DS} is the drain current in the saturation regime, V_{SD} is the drain voltage, W and L are the channel width and channel length respectively, C_i is the capacitance per unit area of the gate dielectric layer, and V_T is the threshold voltage. V_T of the device is determined from the linear relationship between the square root of I_{SD} and V_G in the saturation regime of the transfer characteristics by extrapolating the linear fit to $I_{SD} = 0$. Variable-temperature FET measurements were obtained in a Lakeshore TTP4 probe station under 10^{-6} mbar and recorded by a Keithley 4200-SCS semiconductor parameter analyzer.

Acknowledgements

The authors thank the Institute of Materials Research and Engineering (IMRE), the Agency for Science, Technology and Research (A*STAR), and the Visiting Investigator Program (VIP) for financial support and Mr Poh Chong Lim for assistance with 2D XRD. The authors are also thankful to Lim Shao Xuan, Poh Pei Chi Peggy, Shen Zongmin and Syaza Nur Bte Ishak from Teamasek Polytechnic for their assistance in scaling up some precursors during attachment with IMRE. A portion of this research was conducted at the Center for Nanophase Materials Sciences, which is sponsored at Oak Ridge National Laboratory by the Division of Scientific User Facilities, Office of Basic Energy Sciences, and U.S. Department of Energy.

References

1 A. Dodabalapur, *Mater. Today*, 2006, **9**, 24.
2 *Organic Electronics: Materials, Manufacturing, and Applications*, ed. H. Klauk, WILEY-VCH, Weinheim, Germany, 2006.
3 *Organic Photovoltaics*, ed. C. Brabec, V. Dyakonov, U. Scherf, Wiley-VCH, Weinheim, Germany, 2008.
4 K. Müllen and G. Wegner, *Electronic Materials: The Material Approach*, Wiley-VCH, Weinheim, 1998.
5 S. Allard, M. Forster, B. Souharce, H. Thiem and U. Scherf, *Angew. Chem., Int. Ed.*, 2008, **47**, 4070–4098.
6 A. Facchetti, *Mater. Today*, 2007, **10**, 28.
7 B. S. Ong, Y. Wu, Y. Li, P. Liu and H. Pan, *Chem.–Eur. J.*, 2008, **14**, 4766.
8 Y. Shirota and H. Kageyama, *Chem. Rev.*, 2007, **107**, 953.
9 D. R. Gamota, P. Brazis, K. Kalyanasundaram and J. Zhang, *Printed Organic and Molecular Electronics*, Kluwer Academic Publishers, 2004.
10 J. Roncali, *Chem. Rev.*, 1992, **92**, 711.
11 J. Roncali, *Chem. Rev.*, 1997, **97**, 173.
12 J. Chen and Y. Cao, *Acc. Chem. Res.*, 2009, **42**, 1709.
13 D. Reitzenstein, PhD Dissertation, Julius-Maximillians University, Wurzberg, 2010.
14 A. Facchetti, *Chem. Mater.*, 2011, **23**, 733.
15 B. Tieke, A. R. Rabindranath, K. Zhang and Y. Zhu, *Beilstein J. Org. Chem.*, 2010, **6**, 830.
16 S. Qu and H. Tian, *Chem. Commun.*, 2012, **48**, 3039.
17 L. Bürgi, M. Turbiez, R. Pfeiffer, F. Bienewald, H.-J. Kirner and C. Winnewisser, *Adv. Mater.*, 2008, **20**, 2217.
18 J. C. Bijleveld, A. P. Zoombelt, S. G. J. Mathijssen, M. M. Wienk, M. Turbiez, D. M. de Leeuw and R. A. J. Janssen, *J. Am. Chem. Soc.*, 2009, **131**, 16616.
19 H. Bronstein, Z. Chen, R. S. Ashraf, W. Zhang, J. Du, J. R. Durrant, P. S. Tuladhar, K. Song, S. E. Watkins, Y. Geerts, M. M. Wienk, R. A. J. Janssen, T. Anthopoulos, H. Sirringhaus, M. Heeney and I. McCulloch, *J. Am. Chem. Soc.*, 2011, **133**, 3272.
20 J. C. Bijleveld, R. A. M. Verstrijden, M. M. Wienk and R. A. J. Janssen, *J. Mater. Chem.*, 2011, **21**, 9424.
21 T. L. Nelson, T. M. Young, J. Liu, S. P. Mishra, J. A. Belot, C. L. Balliet, A. E. Javier, T. Kowalewski and R. D. McCullough, *Adv. Mater.*, 2010, **22**, 4617.
22 A. R. Mohebbi, J. Yuen, J. Fan, C. Munoz, M. F. Wang, R. S. Shirazi, J. Seifter and F. Wudl, *Adv. Mater.*, 2010, **23**, 4644.
23 P. T. Wu, F. S. Kim and S. A. Jenekhe, *Chem. Mater.*, 2011, **23**, 4618.
24 J. S. Ha, K. H. Kim and D. H. Choi, *J. Am. Chem. Soc.*, 2011, **133**, 10364.
25 P. Sonar, S. P. Singh, Y. Li, M. S. Soh and A. Dodabalapur, *Adv. Mater.*, 2010, **22**, 5409.
26 P. Sonar, S. P. Singh, Y. Li, Z.-E. Ooi, T.-J. Ha, I. Wong, M. S. Soh and A. Dodabalapur, *Energy Environ. Sci.*, 2011, **4**, 2288.
27 Y. Li, S. P. Singh and P. Sonar, *Adv. Mater.*, 2010, **22**, 4862.
28 T. J. Ha, P. Sonar, B. Cobb and A. Dodabalapur, *Org. Elec.*, 2012, **13**, 136.
29 C. H. Woo, P. M. Beaujuge, T. W. Holcombe, O. P. Lee and J. M. J. Fréchet, *J. Am. Chem. Soc.*, 2010, **132**, 15547.
30 J. C. Bijleveld, B. P. Karsten, S. G. J. Mathijssen, M. M. Wienk, D. M. de Leeuw and R. A. J. Janssen, *J. Mater. Chem.*, 2011, **21**, 1600.
31 Y. Li, P. Sonar, S. P. Singh, W. Zeng and M. S. Soh, *J. Mater. Chem.*, 2011, **21**, 10829.
32 P. M. Beaujuge and J. M. J. Fréchet, *J. Am. Chem. Soc.*, 2010, **133**, 20009.
33 P. Sonar, S. P. Singh, Y. Li, E. L. Williams, M. S. Soh and A. Dodabalapur, *J. Mater. Chem.*, 2012, **22**, 4225.
34 J. Kim, B. Lim, K. J. Baeg, Y. Y. Noh, D. Khim, H. G. Jeong, J. M. Yun and D. Y. Kim, *Chem. Mater.*, 2011, **23**, 4663.
35 B. Lim, J. S. Yeo, D. Khim and D. Y. Kim, *Macromol. Rapid Commun.*, 2011, **32**, 1551.
36 B. Lim, K. J. Baeg, H. G. Jeong, J. Jo, H. Kim, J. W. Park, Y. Y. Noh, D. Vak, J. H. Park and D. Y. Kim, *Adv. Mater.*, 2009, **21**, 2808.
37 G. Zhang, K. Liu, Y. Li and M. Yang, *Polym. Int.*, 2009, **58**, 665.
38 M. Shahid, T. M. C. Ward, J. Labram, S. Rossbauer, E. B. Domingo, S. E. Watkins, N. Stingelin, T. D. Anthopoulos and M. Heeney, *Chem. Sci.*, 2012, **3**, 181.
39 S. Wang, J. C. Tang, L. H. Zhao, R. Q. Png, L. Y. Wong, P. J. Chia, H. S. O. Chan, P. K. H. Ho and L. L. Chua, *Appl. Phys. Lett.*, 2008, **93**, 162103.
40 J.-M. Zhuo, L.-H. Zhao, R. Q. Png, L.-Y. Wong, P. J. Chia, J.-C. Tang, S. Sivaramakrishnan, M. Zhou, E. C.-W. Ou, S.-J. Chua, W. S. Sim, L.-L. Chua and P. K.-H. Ho, *Adv. Mater.*, 2009, **21**, 4747.
41 R. J. Kline and M. D. McGehee, *Polym. Rev.*, 2006, **46**, 27.
42 I. McCulloch, M. Heeney, C. Bailey, K. Genevicius, I. Macdonald, M. Shkunov, D. Sparrowe, S. Tierney, R. Wagner, W. M. Zhnag, M. L. Chabinyc, R. J. Kline, M. D. Mcgehee and M. F. Toney, *Nat. Mater.*, 2006, **5**, 328.
43 H. W. Lin, W. Y. Lee and W. C. Chen, *J. Mater. Chem.*, 2012, **22**, 2120.

